AgriEngineering

Article

Microwave-Induced Thermal Inactivation of *Fusarium solani* Strain Isolated from Cocoa Pods: Experimental Determination of the Temperature Threshold for Fungal Lethality

William A. Lombana Peña [1], Omar A. Nova Manosalva [1,*], Hector F. Guarnizo-Mendez [2], Nuri Andrea Merchán Castellanos [3] and Andrés Polochè Arango [1]

[1] Faculty of Engineering and Basic Sciences, Fundación Universitaria Los Libertadores, Bogotá 111221, Colombia; wlombanape@libertadores.edu.co (W.A.L.P.); andres.poloche@libertadores.edu.co (A.P.A.)
[2] Electronics Engineering Department, Universidad El Bosque, Bogotá 111321, Colombia; hguarnizo@unbosque.edu.co
[3] Bioengineering Department, Universidad El Bosque, Bogotá 111321, Colombia; nmerchanc@unbosque.edu.co
* Correspondence: oanovam@libertadores.edu.co

Abstract

Cocoa (*Theobroma cacao* L.) postharvest quality can be compromised by fungal colonization across the farm-to-chocolate continuum, motivating non-chemical control options that can be engineered as unit operations. This study evaluates microwave (MW) irradiation (2.45 GHz) as a physical disinfestation process against *Fusarium solani* (*F. solani*). Experiments were conducted under a completely randomized design (CRD) by tuning MW power (140–210 W) and exposure time to reach predefined surface-temperature bands verified by infrared (IR) thermography. Post-treatment viability was assessed by incubation (27 °C, 7–10 days) and classified as Reduced Growth Rate (RGR; sublethal regrowth slower than control) or Death (D; no regrowth comparable to autoclaved negative controls). Outcomes were temperature-governed: RGR predominated in sublethal bands (60–80 °C), whereas consistent D occurred once surface temperature exceeded 80 °C. Thermodynamic modeling established a median lethal temperature (LT_{50}) of 81.0 °C, and a 99% eradication threshold (LT_{99}) of 87.2 °C. Maximizing the heating rate (H_r) to 0.381 °C/s at 210 W ensured rapid and profound cellular suppression. Scanning electron microscopy (SEM) corroborated severe ultrastructural damage (collapsed macroconidia and disrupted hyphae) under lethal conditions, and turbidimetric monitoring over 120 h showed sustained growth suppression in treated samples. These findings define a practical lethal threshold and power–time windows to inform MW scale-up as a postharvest unit operation while minimizing thermal residence time.

Keywords: cocoa; *Fusarium solani*; microwave irradiation; postharvest disinfestation; infrared thermography; thermal inactivation; power–time treatment adjustment; process kinetics; continuous processing; scanning electron microscopy

Academic Editor: Gabriel Henrique Horta de Oliveira

Received: 21 July 2026
Revised: 11 September 2026
Accepted: 14 September 2026
Published: 20 September 2026

1. Introduction

Cocoa (*Theobroma cacao* L.) is exposed to complex fungal communities along the farm-to-postharvest continuum, and these communities can compromise quality and value along the supply chain [1,2]. Within these communities, the *F. solani* species complex (FSSC) is a ubiquitous and agriculturally important pathogen group comprising at least

60 phylogenetically distinct species [3]. FSSC virulence is linked to dynamic genome biology, including dispensable (supernumerary) chromosomes that can contribute to heterogeneity in aggressiveness and ecological fitness [3]. More broadly, *Fusarium*-induced diseases are recognized as recurring constraints in tropical perennial cropping systems, reinforcing the need for scalable control options beyond field-only interventions [4]. In fact, recent integrative genomic and pathogenicity analyses explicitly identify these *Fusarium* species complexes as emerging and critical threats to cacao (*Theobroma cacao*) cultivation, driving the exploration of advanced physical disinfection platforms [5].

Within the cocoa production chain, the phytopathogenic fungus *F. solani* generates critical damage by attacking the base of the plants, root systems, and vascular tissues. Upon colonizing the internal tissues, the pathogen obstructs the efficient transport of water and essential nutrients, manifesting externally as generalized wilting, loss of turgor, and progressive chlorosis [6]. Furthermore, strains of the *F. solani* species complex are associated with severe pod rot during harvest and postharvest storage [7], interacting with other fungal pathogens to drastically degrade internal bean quality [8].

Microwave (MW) irradiation is a promising non-chemical physical control method because it can deliver rapid thermal energy and be engineered as a unit operation. Reviews and recent syntheses emphasize that MW inactivation depends strongly on process conditions, moisture, and matrix properties, and therefore should be specified using measurable thermal endpoints rather than exposure time alone [9–12]. Consistent with this framework, MW efficacy has been reported for agri-food disinfestation; for example, it reduced fungal colonization in Brazil nut shells and kernels [13]. In fruit systems, MW has been investigated for postharvest fungal rot control, including stand-alone MW and MW combined with antagonistic yeasts [14]. In seed and propagation contexts, MW and MW-adjacent approaches have been evaluated to mitigate seedborne pathogen pressure, including onion seed-associated pathogens and *Fusarium oxysporum* f. sp. *melonis* during commercial production of melon plantlets [15,16].

Beyond cocoa, MW-based fungal control has been explored in fruit and nut systems, including aflatoxin-related contexts, supporting MW as a broader postharvest control platform [14,17]. In cereal matrices, recent reviews and comparative studies discuss electromagnetic/MW approaches to limit fungal spoilage and related safety risks, reinforcing the importance of process variables and matrix effects when defining lethal conditions [11,12,18,19].

Translating MW to cocoa requires explicit attention to plant-matrix complexity. MW effectiveness depends on dielectric properties, and differential heating can emerge in heterogeneous plant materials [13,20]. Related dielectric measurements in infected plant residues further support that dielectric heterogeneity can shape MW interactions and heating patterns in biological substrates [21]. Moreover, pathogen robustness and structural barriers matter: matrix-dependent outcomes reported for silver nanoparticle (AgNP) treatments in cocoa highlight that antifungal efficacy can differ substantially between simplified media and plant tissues, motivating validation strategies that separate superficial injury from true loss of viability [22].

Importantly, MW processing is already embedded in the cocoa value chain through roasting and multiple MW-assisted processing/valorization routes for cocoa materials and residues [20,23–29]. In parallel, MW-enabled process intensification can generate antifungal bioactives; for example, ultrasound–microwave polyphenolic extracts have shown activity against *F. solani* [30].

To address this gap, we evaluated MW irradiation (2.45 GHz) as a physical disinfestation process against *F. solani* under a completely randomized design (CRD). MW power (140–210 W) and exposure time were adjusted to reach predefined surface-temperature

bands verified by infrared (IR) thermography. Post-treatment viability was assessed after incubation (27 °C, 7–10 days) and categorized as reduced growth rate (RGR) or death (D) using untreated and autoclaved controls as benchmarks. Structural corroboration of lethality was obtained by scanning electron microscopy (SEM) of macroconidia and hyphae under lethal conditions, and persistence of growth suppression was monitored turbidimetrically over 120 h.

Despite MW applications across commodities and configurations, cocoa-focused evidence remains limited regarding temperature-verified lethal thresholds and practical power–time windows for *F. solani* under cocoa-relevant conditions. Therefore, this study aims to define a temperature-governed lethal threshold and design-relevant power–time windows for MW-based control of *F. solani*, supported by thermography and ultrastructural validation.

The Graphical Abstract summarizes the experimental workflow used to evaluate microwave-induced thermal inactivation of *F. solani* isolated from infected cocoa pods. The fungal isolate was cultured under controlled conditions (27 °C for 7–10 days) to obtain viable fungal material, which was subsequently exposed to microwave irradiation at 2.45 GHz. During treatment, surface temperature was continuously verified using infrared thermography to establish the relationship between microwave exposure, heating, and fungal viability. The effects of the treatment were subsequently assessed through scanning electron microscopy (SEM), revealing clear morphological alterations in treated macroconidia, including loss of structural integrity, shrinkage, and surface collapse. The temperature–response analysis showed that exposure within the 60–80 °C range primarily resulted in a reduced growth rate (RGR), whereas temperatures above 80 °C produced fungal death (D), and the sample becomes charred above 100 °C. In addition, the comparison of heating demonstrated that higher microwave power increased the rate at which the lethal temperature threshold was reached. Overall, the graphical abstract highlights that temperature governs fungal lethality, while microwave power primarily governs heating rate, supporting microwave irradiation as a potential non-chemical strategy for postharvest control of *F. solani* in cocoa.

2. Materials and Methods

2.1. Biological Material

The test fungal organism was *F. solani*, identified as the etiological agent of cocoa pod rot (*Theobroma cacao* L.). The isolation source consisted of infected pods collected directly from the field, ensuring the virulence and representativeness of the local strain. Plant tissues were initially washed under running tap water to remove adhering soil particles and debris, followed by rinsing with sterile distilled water. Samples were surface-sterilized by immersion in 70% ethanol for 1 min and rinsed three times with sterile distilled water. Tissue fragments (approximately 5 mm × 5 mm) were aseptically excised and placed onto PDA plates supplemented with chloramphenicol (100 mg L^{-1}). The inoculated plates were incubated at 27 °C for 7–10 days and monitored daily for fungal growth. Emerging fungal colonies were subcultured onto fresh PDA plates using hyphal-tip transfer until pure cultures were obtained.

To confirm the virulence of the CHA1 isolate, an in vivo pathogenicity assay was conducted on healthy, detached cocoa pods (*Theobroma cacao* L.). The pods were surface-sterilized (70% ethanol) and inoculated via syringe injection with a standardized conidial suspension (1.6×10^8 conidia mL^{-1}) directly into the mesocarp (Figure 1a). Inoculated pods were incubated in a humid chamber (27 °C, 85–90% RH) and monitored daily. Consistent with pathological descriptions for Fusarium species complexes affecting cacao tissues, the infection initiated as moist, dark-brown to black lesions near the inoculation site. These

symptoms exhibited progressive expansion across the cuticular surface, followed by dense white-to-cottony mycelial proliferation under high humidity, ultimately leading to tissue dehydration and mummification by day 26 (Figure 1b,c) [5]. The pathogen was successfully re-isolated from the advancing lesion margins, fulfilling Koch's postulates and confirming active virulence.

(**a**) (**b**) (**c**)

Figure 1. In vivo pathogenicity assay on detached cocoa pods (*Theobroma cacao* L.) to experimentally confirm the virulence of the isolated *F. solani* CHA1 strain. (**a**) Direct syringe inoculation of a standardized conidial suspension (1.6×10^8 conidia mL^{-1}) into the mesocarp (Day 0). (**b**) Initial necrotic lesion development observed 15 days post-inoculation. (**c**) Severe necrotic expansion and external mycelial colonization 26 days post-inoculation, fulfilling Koch's postulates.

2.2. Materials and Equipment

Equipment and consumables were selected based on the requirement to generate controlled electromagnetic radiation and perform precise ultrastructural analyses.

The central apparatus was a laboratory microwave oven (Brand: KALLEY, Model: K-MW07N, Kalley, Medellín, Colombia, cavity dimensions: 31.5 cm width × 20.5 cm height × 29.5 cm depth) operating at a fixed frequency of 2.45 GHz. Samples were positioned exactly in the center of the oven on a rotary plate to ensure a uniform distribution of the electromagnetic heating. Preliminary trials evaluated four power levels: 70, 140, 210, and 280 W. The 70 W setting was discarded because the heating was excessively slow and failed to reach the required thermal thresholds, while the 280 W setting caused immediate sample carbonization. Consequently, 140 W and 210 W were selected as the standardized power levels for all experiments.

For microbiological quality control and media preparation, a vertical autoclave was used for sterilization and to generate sterile negative controls. The evaluation of radiation-induced structural damage was conducted via Scanning Electron Microscopy (SEM) using a Carl Zeiss EVO HD15 system, Carl Zeiss AG, Oberkochen, Germany.

Monitoring secondary thermal effects was essential; thus, a portable thermal camera (HURRICANE, model 02-053, Jiangsu Sainty Sumex Tools Corp. Ltd., Nanjing, China) was employed to record the distribution and kinetics of the surface temperature. The device features a measurement uncertainty of ±2 °C (or ±2%), a temporal resolution of 9 Hz, and a 32 × 32 infrared pixel resolution. To ensure measurement accuracy, the emissivity parameter was manually calibrated to 0.95, which is the established thermodynamic standard for highly aqueous organic materials and biological matrices (such as fungal tissue and agar media) that closely approximate ideal black-body radiation. Finally, 90 mm diameter sterile Petri dishes, automatic pipettes (Eppendorf®, Eppendorf SE, Hamburg, Germany), and sterile tips were used for the aseptic handling of inocula, PDA culture media, and Nutrient Agar for the propagation and subsequent evaluation of the fungus's cellular viability. Additionally, healthy cocoa pods *Theobroma cacao* L. were collected from the experimental farm to serve as a substrate for future pathogenicity assays.

2.3. DNA Extraction

The entire fungal mycelial biomass from a colonized Petri dish culture was harvested and used for DNA extraction. The harvested mycelium was transferred to a microcentrifuge tube containing 700 µL of lysis buffer (1 M KCl, 100 mM Tris-HCl, and 10 mM EDTA) and glass beads. Mechanical cell disruption was performed using a FastPrep homogenizer (MP Biomedicals, Solon, OH, USA) with three cycles at 40 m s^{-1} for 5 s per cycle. Following cell lysis, samples were centrifuged at 5.000 rpm for 10 min to remove cellular debris. The resulting supernatant was transferred to a new tube and mixed with 300 µL of isopropanol by gentle inversion to precipitate nucleic acids. Samples were then centrifuged at 12.000 rpm for 10 min, and the resulting DNA pellet was washed with 800 µL of 70% ethanol. After washing, samples were centrifuged at 12.000 rpm for 3 min, and the ethanol was carefully discarded. Residual ethanol was allowed to evaporate completely at room temperature. Finally, the DNA pellet was resuspended in 100 µL of molecular-grade water and stored at −20 °C.

PCR Amplification and Phylogenetic Analysis

Molecular identification of the fungal isolates was performed through the amplification of the internal transcribed spacer (ITS) region and the large subunit ribosomal RNA (LSU rRNA) gene. The ITS region was amplified using the primer pair ITS1 (5′-CTTGGTCATTTAGAGGAAGTAA-3′) and ITS4 (5′- GGAAGTAAAAGTCGTAACAAGG-3′) [31], whereas the LSU region was amplified using the primers LR0R (5′- ACCCGCTGAAC TTAAGC-3′) and LR5 (5′- ATCCTGAGGGAAACTTC-3′) [32]. PCR amplifications were carried out following the protocol described by [31]. PCR products were sequenced and compared against reference sequences available in public databases for taxonomic identification.

The phylogenetic analyses were performed using Geneious Prime® 2026.1.2 software based on the neighbor-joining method, inferred from LSU rDNA sequence data. Multiple sequence alignments were generated using the MUSCLE algorithm. The reliability of the inferred phylogenetic relationships was assessed by bootstrap analysis with 1000 replicates. The phylogenetic tree was rooted using *Fusarium* staphyleae NRRL 22316 (GenBank accession AF178392) as the outgroup.

2.4. Adjustment of Times to Obtain Pre-Established Temperatures

The experiment was conducted under a Completely Randomized Design (CRD) with three replicates per treatment. The primary factors evaluated were the electromagnetic radiation power, set at levels of 140 W and 210 W, and the exposure times, which were adjusted based on preliminary trials to reach four surface temperature ranges: 60–70 °C, 70–80 °C, 80–90 °C, and 90–100 °C. To ensure assay validity, two control treatments were established: a positive control (+), consisting of viable spores without radiation exposure, and a negative control (−), comprising spores inactivated by autoclaving at 120 °C for 15 min at 15 PSI.

The experimental design for microwave thermal exposure and sample manipulation was adapted from established electromagnetic disinfestation methodologies previously validated for agricultural substrates [33–35].

Exposure of Samples to Microwave Radiation

Mycelial plugs (with average dimensions of 5 mm in length and 2 mm in diameter) were extracted from active *F. solani* colonies using a sterile cork borer. These discs were placed in Petri dishes with fresh PDA medium and positioned individually in the centre of the microwave oven to ensure a uniform distribution of electromagnetic energy.

During treatment application, the exposure times required to reach the pre-established temperature ranges were strictly followed, monitoring surface temperature kinetics at regular intervals using a portable thermal camera calibrated in degrees Celsius (°C). Following exposure, treated samples were incubated at 27 °C for 7–10 days in complete darkness. After this period, the effect of radiation on fungal viability was classified into two categories: Death (D), defined by the total absence of fungal growth; and Reduced Growth Rate (RGR), in cases where mycelial development was evident but at a significantly lower rate than that observed in the positive control.

2.5. Methodology for Determining Conidial Survival Kinetics

The fungal isolate *F. solani* was cultured on Potato Dextrose Agar (PDA) plates and incubated at 27 °C for 7–10 days to promote mycelial growth and sporulation. A conidial suspension was prepared by harvesting conidia from sporulating culture with 0.1% peptone water and Tween 80 (0.01%). The suspension was filtered to remove large mycelial aggregates when necessary. The conidial concentration was determined using a Neubauer hemocytometer and adjusted with sterile peptone water to obtain a final concentration of 1.6×10^8 conidia mL^{-1}.

Aliquots of the standardized conidial suspension were exposed to microwave radiation treatments at power levels of 140 W and 210 W, with exposure times adjusted to reach four target surface temperature ranges: 60–70 °C, 70–80 °C, 80–90 °C, and 90–100 °C. Meanwhile, untreated suspensions of viable spores served as a positive control, and spores inactivated by autoclaving at 120 °C for 15 min served as a negative control. The conidial suspension was inoculated into Potato Dextrose Broth (PDB) and incubated at 28 °C. *F. solani* growth was monitored over time by measuring the optical density (OD) at 600 nm (OD600) at 0, 24, 48, 72, 96, and 120 h of incubation [36].

To quantify the post-treatment efficacy, the absolute difference in optical density (ΔOD) between the untreated control and the microwave-treated samples was calculated. The cellular inhibition percentage (%) was determined based on this difference relative to the maximum growth of the control at each time point.

2.6. Sample Preparation for SEM

To evaluate the ultrastructural alterations induced by electromagnetic and thermal treatments, the fungal isolate was initially grown for 15 days on PDA medium at 27 °C to promote sporulation. Subsequently, the spores were harvested by washing with a 0.1% Tween 80 solution. The collected spores were quantified using a Neubauer hemocytometer, and the concentration was adjusted to 1.6×10^8 conidia mL^{-1}. For microwave radiation exposure, 30 µL/mL of the spore suspension was utilized. Following the treatments, the spores and mycelial structures underwent a rigorous fixation and dehydration protocol.

Initially, samples were fixed in a 2.5% glutaraldehyde solution for 24 h. Subsequently, post-fixation was performed using 1% osmium tetroxide, followed by successive washes with phosphate buffer to remove residual fixative agents. The samples then underwent a chemical drying process using hexamethyldisilazane (HMDS) and were finished with a gold-palladium coating to optimize conductivity. Topographic observation and analysis were performed using a Carl Zeiss EVO HD15 scanning electron microscope (SEM) at magnifications up to 10,000×. The evaluation consisted of a detailed comparison of micrographs from the treatments against the controls, paying particular attention to cell wall integrity, variations in spore morphology, and the presence of evident signs of structural collapse.

It is important to note that all samples designated for SEM analysis were collected and fixed immediately following microwave irradiation to capture the acute structural impact. Additionally, a quantitative morphometric analysis of fungal structures was performed on

the acquired SEM micrographs using the established image scale bar (2 µm) as a spatial calibration reference ($k = 0.0290 \pm 0.0008$ µm/px). For both the untreated control and the irradiated samples, a representative sample of individual spores ($n = 12$ per group) was measured to determine their longitudinal length (major axis) and transverse width (minor axis).

2.7. Evaluation of Radial Growth Kinetics and Fungal Inhibition

To determine the impact of electromagnetic treatments on the viability and germinative vigour of *F. solani*, its macroscopic in vitro development was evaluated. Aliquots from previously irradiated spore suspensions were aseptically inoculated into the centre of Petri dishes. Two solid culture media were used for this assay: PDA and Nutrient Agar. The plates were then incubated under controlled temperature conditions and in strict darkness to favour pathogen development.

While radial expansion on solid media was qualitatively observed to confirm the presence or absence of macroscopic viability, the rigorous quantitative evaluation of fungal inhibition and cellular vigour was determined exclusively through the turbidimetric absorbance (OD_{600}) of the liquid cultures over time, as detailed in Section 2.5.

2.8. Heat Transfer Kinetics and Energy Rate

To evaluate the energy transfer efficiency of the microwave treatments and its physical impact on fungal inactivation, the thermal kinetics were analyzed, and the heating rate (H_r) was quantified during the initial linear thermal ascent phase. The speed at which the biological matrix absorbs electromagnetic energy is a critical engineering factor for minimizing stress-adaptive responses in pathogens [37]. The heating rate was calculated using the following equation:

$$H_r = \frac{T_f - T_i}{t_f \times 60}$$

where H_r is expressed in °C/s; T_f is the surface temperature upon stabilization of the linear ascent phase (°C); T_i is the standardized initial temperature (20 °C); and t_f is the required exposure time converted to seconds. All experiments were conducted using a completely randomized design (CRD). Data were expressed as the mean ± standard deviation.

2.9. Statistical Analysis and Thermodynamic Modeling

All in vitro experiments evaluating *F. solani* were conducted under a completely randomized design (CRD). To rigorously validate the biological efficacy and thermodynamic engineering parameters, the statistical analysis prioritized formal hypothesis testing and predictive modeling over observational data dispersion. Consequently, the analytical hierarchy was established as follows: (1) One-way ANOVA as the primary test to determine significant differences in overall viability; (2) Pearson correlation to establish the linear relationship between thermal load and suppression; (3) Binomial Logistic Regression, including model fit evaluation and 95% Confidence Intervals (CI), to mathematically derive lethality thresholds; and finally, (4) the separation of Standard Deviation (SD) bars as a supplementary visual indicator of biological variance. The specific variables defined for each model are detailed in Table 1.

Prior to mean comparisons, data normality was verified using the Shapiro–Wilk test. Subsequently, dimensional changes (spore length and width) obtained from the SEM morphometric analysis were compared between the untreated control and the microwave-treated group using an independent-samples Student's *t*-test ($p < 0.05$).

Table 1. Summary of the statistical design, defining the independent and dependent variables for each test.

Statistical Test	Independent Variable (Predictor)	Dependent Variable (Response)	Primary Purpose
One-way ANOVA	Treatment Category (Untreated Control vs. Microwave-Treated)	Fungal Viability (OD_{600} absorbance across 120 h, $n = 11$)	To determine statistically significant macroscopic suppression.
Pearson Correlation	Maximum Surface Temperature Achieved (°C)	Cellular Inhibition (%)	To quantify the linear relationship between heat and biological response.
Binomial Logistic Regression	Maximum Surface Temperature Achieved (°C)	Binary Biological Outcome (0 = RGR, 1 = Macroscopic Death [D])	To mathematically derive the LT_{50} and LT_{99} thermal thresholds.

3. Results

3.1. Molecular Identification and Phylogenetic Analysis

Molecular identification based on the LSU rDNA sequence showed a high degree of similarity between the isolate CHA1 (recovered from infected cocoa pods) and members of the *F. solani* species complex. BLASTn analysis of the 723-bp LSU sequence showed 99.86% sequence identity and 100% query coverage with Fusarium cf. solani isolate CRSFA.Fus.04 (GenBank OQ818664.1), with one mismatch, no gaps, and an E-value of 0.0. The sequence also showed 99.86% identity and 100% query coverage with a sequence identified as *F. solani* (KJ126623.1). Phylogenetic analysis based on LSU rDNA further placed the isolate within the *F. solani* species complex, robustly supporting its affiliation with this group (Figure 2).

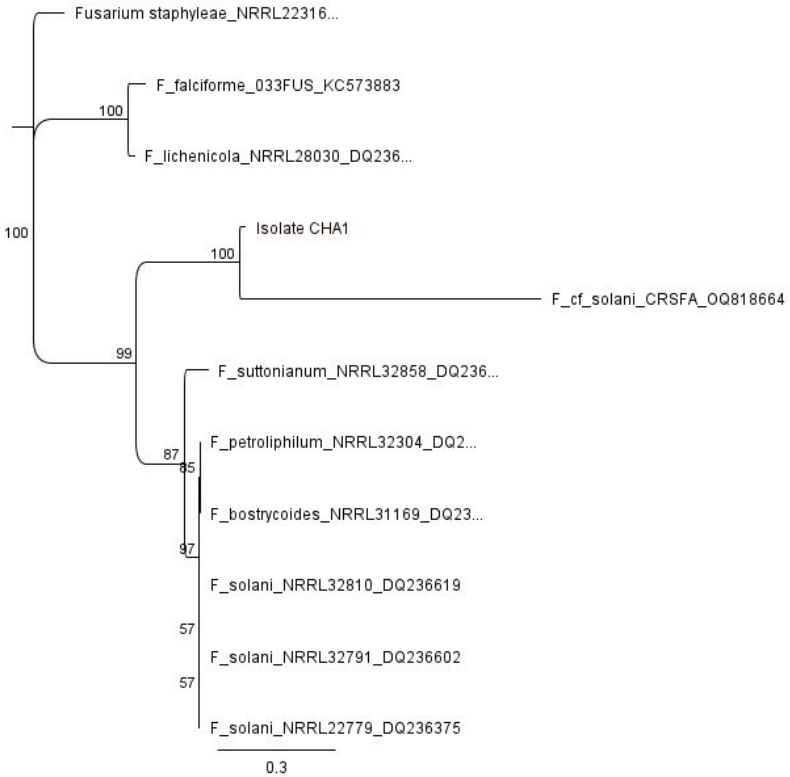

Figure 2. Phylogenetic analysis of Fusarium solani CHA1 isolated from cocoa pods using LSU rDNA sequence. The phylogenetic analyses were performed using Geneious Prime® 2026.1.2 software with the Neighbor-Joining method. The analysis included 11 nucleotide sequences, with Fusarium staphyleae NRRL 22316 used as the outgroup. Numbers displayed at the internal nodes indicate bootstrap support values based on 1000 replicates; only values above 50% are shown. The scale bar represents 0.3 nucleotide substitutions per site.

The LSU rDNA sequence of the CHA1 isolate generated in this study was deposited in the GenBank database under the accession number [SUB16465969].

3.2. Thermal Kinetics and Electromagnetic Lethality Against F. solani

Thermal kinetics (temperature vs. time) and their effect on pathogen viability were evaluated under a completely randomized design (CRD). The biological response was classified as Reduced Growth Rate (RGR) or Death (D). Analysis of the interaction between microwave power and exposure time revealed the following thermotolerance dynamics across the target surface temperature ranges:

Sublethal tolerance zone (60–80 °C):

The thermal energy transferred within the 60–70 °C and 70–80 °C bands was biologically insufficient to induce complete lethality. Samples within these ranges exhibited RGR. The treatment induced significant metabolic stress and delayed colonization, but allowed survival and debilitated recovery, confirming that temperatures up to 80 °C constitute a sublethal stress environment for this specific strain.

Severe inactivation and thermal shock (>80 °C):

Progression to higher ranges (80–90 °C and 90–100 °C) consolidated complete inoculum destruction, with 100% of replicates classified as Death (D). The 210 W treatment showed superior kinetic efficiency, reaching near-boiling temperatures rapidly and inducing an acute thermal shock that prevented any adaptive response.

3.3. Conidial Survival Kinetics

Fungal growth kinetics and quantification of cellular stress:

Turbidimetric monitoring of *F. solani* development over an extended period of 120 h enabled objective quantification of the long-term efficacy of the electromagnetic treatment. The absorbance curves reveal a profound alteration in the pathogen's population dynamics, where the inclusion of standard deviation bars highlights both the biological response and the consistency of the treatment (Figure 3).

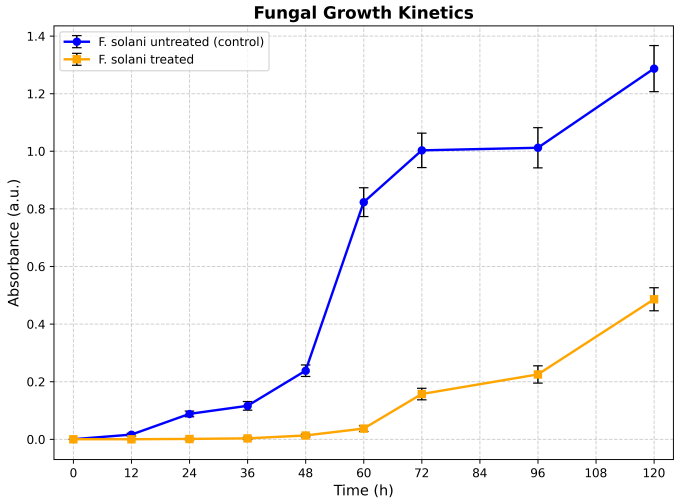

Figure 3. Turbidimetric monitoring of *F. solani* growth over 120 h. The untreated control exhibits a typical kinetic pattern. The microwave-treated condition (represented by the 210 W treatment targeting the 80–90 °C thermal window; maximum exposure time ≈ 17 min) shows drastic and sustained growth suppression, registering an average optical density of OD = 0.486 ± 0.077 at 120 h. The complete separation of the standard deviation bars during the critical exponential phase confirms the significant long-term efficacy of the treatment. Error bars represent the standard deviation of three replicates per treatment.

Growth dynamics and data variability:

Analysis of the positive control curve showed the characteristic kinetic behavior of a highly viable strain. After a natural lag phase of approximately 24 h, the fungus entered an accelerated logarithmic growth phase. During the early exponential growth phase (48 h to 72 h), the untreated control exhibited substantial biological variability, evidenced by large standard deviation bars that overlap with those of the treated samples. By 120 h, this vigorous and sustained proliferation reached a high optical density ($OD > 1.2$), confirming the optimal germination capacity of the original inoculum (Figure 3).

Sustained inhibitory effect (120 h):

In marked contrast, the electromagnetically treated samples exhibited a drastic suppression of growth over the 5-day period (averaging $OD = 0.486$ at 120 h compared to 1.287 in the untreated control) (Figure 3). Although a severely debilitated recovery is observed by the end of the monitoring period ($OD \approx 0.49$), the visual separation of the standard deviation (SD) bars from the control provides supplementary observational evidence of this long-term suppression. However, the formal validation of this efficacy is strictly supported by the subsequent inferential statistics (ANOVA and regression models).

As detailed in Table 2, the microwave treatment induced a peak cellular inhibition of 94.5% during the early exponential phase (48 h), which gradually transitioned to 62.2% by 120 h, demonstrating a severe but progressively stabilizing suppression of fungal vigor.

Table 2. Turbidimetric growth tracking and cellular inhibition of *F. solani* over 120 h post-microwave treatment (expanded time series, $n = 11$).

Time (h)	Untreated Control (Mean (OD_{600}))	Microwave-Treated (Mean (OD_{600}))	Difference (ΔOD)	Inhibition (%)
0	0.000	0.000	0.000	0
12	0.060	0.003	0.056	94
24	0.119	0.007	0.113	95
36	0.179	0.010	0.169	95
48	0.238	0.013	0.225	95
60	0.621	0.085	0.536	86
72	1.003	0.157	0.846	84
84	1.097	0.233	0.864	79
96	1.145	0.322	0.824	72
108	1.216	0.404	0.812	67
120	1.287	0.486	0.801	62

Note: The cellular inhibition percentage was calculated based on the difference (ΔOD) relative to the progressive proliferation of the untreated control.

3.4. Heating Rate (H_r) and Statistical Validation of Fungal Suppression

Thermal kinetics analysis (Table 3) revealed that irradiation power directly governs the heat transfer rate (H_r). The integration of these heating rates with the biological outcomes confirmed the robust efficacy of the microwave unit operation. As illustrated in Figures 4 and 5, operating at 140 W generated moderate heating rates (e.g., 0.085 to 0.164 °C/s), resulting in prolonged exposures within the sublethal ranges (60–80 °C) where the fungus only exhibited a Reduced Growth Rate (RGR).

Statistically, the evaluation of the aggregated optical density data across the monitoring period prioritized formal hypothesis testing. Using the treatment condition as the independent categorical variable and the OD_{600} absorbance as the continuous dependent variable ($n = 11$ observations per group), a one-way ANOVA validated that microwave irradiation significantly suppressed overall *F. solani* viability compared to the untreated control ($F = 8.1744$, $p = 0.0097$, Table 4).

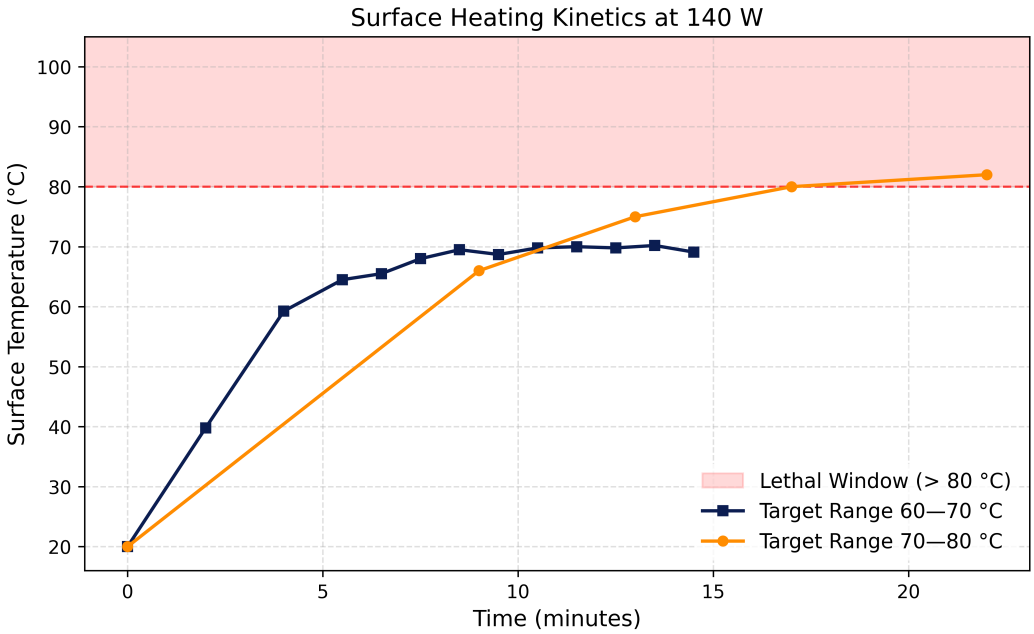

Figure 4. Surface thermal profiles of *F. solani* samples under continuous microwave irradiation at 140 W. The dark blue line represents the averaged temperature profile ($n = 3$) for the 60–70 °C target range. The orange line represents the trajectory for the 70–80 °C target range. The red dashed line and shaded area indicate the lethal thermal window (>80 °C). At 140 W, both thermal profiles remain primarily below the lethal threshold, resulting in sublethal stress (RGR).

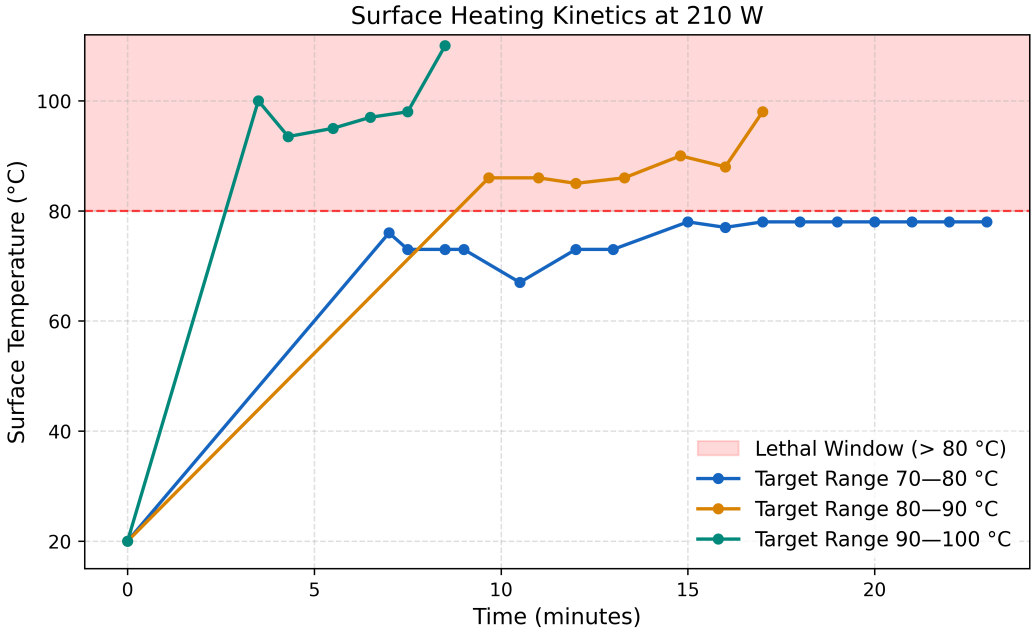

Figure 5. Surface thermal profiles of *F. solani* samples under continuous microwave irradiation at 210 W. The high-power treatments induce a rapid volumetric temperature increase, aggressively crossing into the lethal thermal window (>80 °C, red shaded area) in shorter exposure times. This acute thermal shock consistently correlates with severe structural collapse and suppression (D).

Table 3. Results of thermal analysis and its biological impact.

Power (W)	Target Range (°C)	Linear Ascent Time (t_f) (min)	Final Temp. Achieved (T_f) (°C)	Heating Rate (H_r) (°C/s)	Biological Outcome
140 W	60–70	4.00	59.25 ± 3.10	0.164 ± 0.012	RGR (Sublethal)
140 W	70–80	9.00	66.00	0.085	RGR (Sublethal)
210 W	70–80	7.00	76.00	0.133	RGR (Sublethal)
210 W	80–90	9.67	86.00	0.114	D (Lethal)
210 W	90–100	3.50	100.00	0.381	D (Thermal Shock)

The initial temperature (T_i) for all assays was set at 20 °C at time $t = 0$. For all treatments, values represent the average of 3 experimental replicates ($n = 3$) ± their standard deviation. The biological outcome assumes a reduced growth rate (RGR) for thermal profiles that failed to exceed the macroscopic lethality threshold of 80 °C, and a severe structural collapse and suppression (D) for treatments that effectively crossed this threshold.

Table 4. Analysis of Variance (ANOVA) for overall fungal viability (OD_{600}) across the monitoring timeline.

Source of Variation	DF	Sum of Squares (SS)	Mean Square (MS)	F-Statistic	*p*-Value
Between Groups (Treatments)	1	1.2503	1.2503	8.1744	0.0097
Within Groups (Error)	20	3.0590	0.1529		
Total	21	4.3092			

The lower variance observed in the treated group (0.0320) compared to the untreated control (0.2738) confirms that the electromagnetic intervention effectively constrains population proliferation.

Following the ANOVA, a Pearson correlation analysis utilizing the maximum surface temperature achieved across the critical thermal range (76 °C to 100 °C) as the independent variable and the percentage of cellular inhibition as the dependent variable mathematically confirmed a highly significant positive relationship ($r = 0.9794$, $p = 0.0006$) (Figure 6). The separation of the standard deviation bars observed in the growth kinetics (Figure 3) serves as a supplementary visual representation of this profound biological suppression.

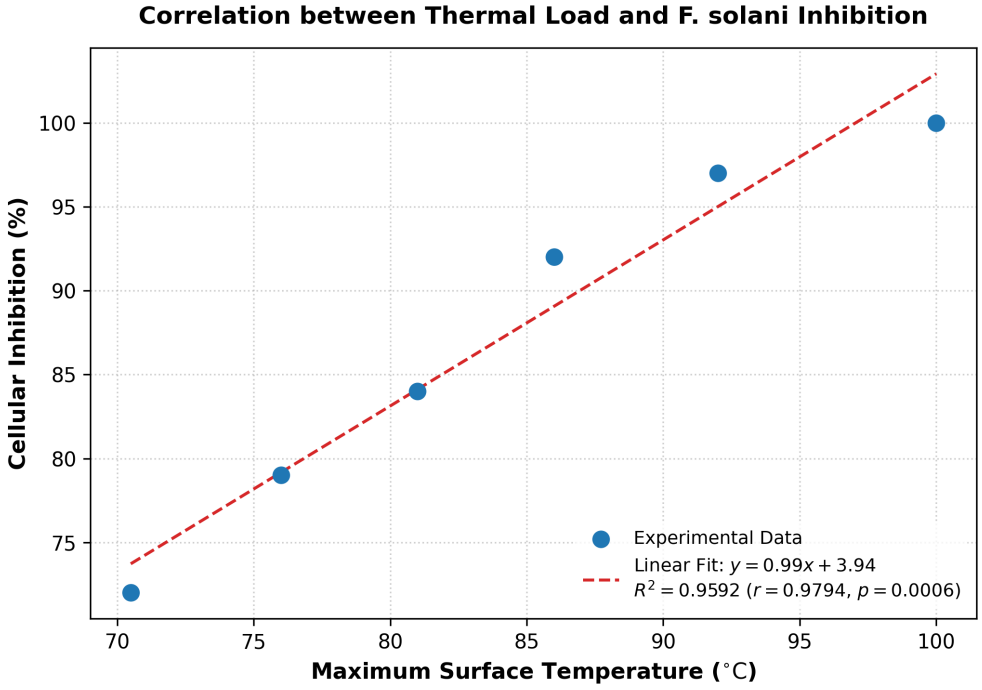

Figure 6. Linear correlation between maximum surface temperature and cellular inhibition percentage of *F. solani* across the critical thermal range (76 °C to 100 °C).

3.5. Logistic Regression and Lethal Thermal Indices

While the Pearson correlation established a linear trend for thermal accumulation, the binomial logistic regression precisely modeled the biological breaking point (Figure 7). By utilizing the maximum surface temperature (°C) as the continuous independent predictor and the biological outcome (0 = RGR, 1 = D) as the binary dependent variable, the logistic model demonstrated an exceptionally strong fit to the experimental data. To evaluate this goodness-of-fit, McFadden's pseudo-R^2 was calculated, yielding a value of 0.9592 ($p < 0.001$). This metric confirms that nearly 96% of the variance in the fungal suppression probability is directly explained by the achieved surface temperature, indicating a highly reliable predictive model.

To rigorously quantify the uncertainty of these predictions, 95% Confidence Intervals (CI) were calculated for the critical thermodynamic thresholds. The regression established that the median lethal temperature (LT_{50})—required to achieve a 50% probability of severe cellular suppression—is located at 81.0 °C (95% CI: 79.2–82.8 °C). Furthermore, the threshold for 99% probabilistic suppression (LT_{99}) is mathematically projected at 87.2 °C (95% CI: 85.1–90.4 °C). The narrow bounds of these confidence intervals demonstrate low statistical uncertainty, numerically validating that disinfestation units must be engineered with sufficient power (e.g., 210 W) to rapidly push the surface temperature beyond the 80 °C barrier.

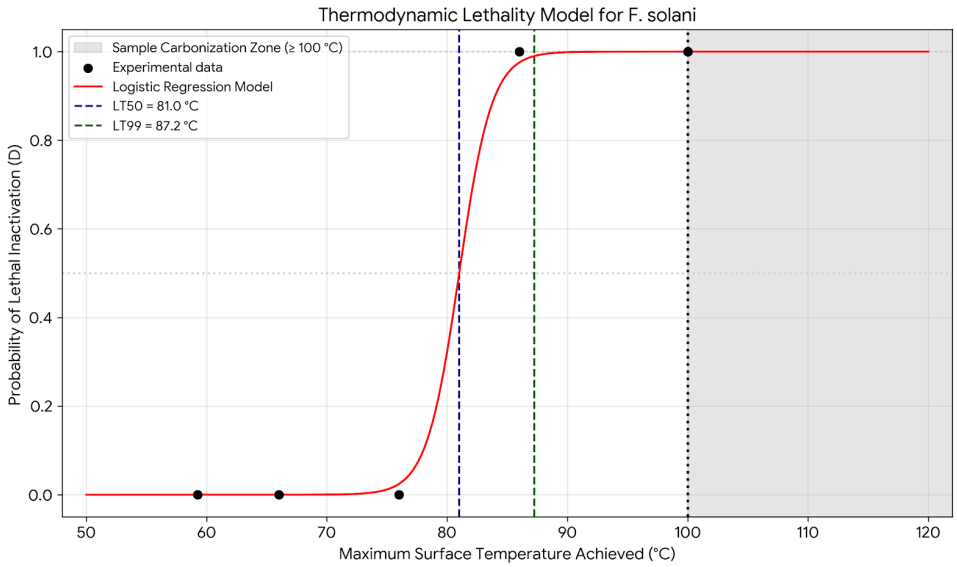

Figure 7. Binomial logistic regression model predicting the thermal inactivation probability of *F. solani* as a function of the maximum surface temperature achieved via microwave irradiation. The solid red line represents the fitted probability curve. Experimental biological outcomes (black dots) are coded as (0) for sublethal Reduced Growth Rate (RGR) and (1) for macroscopic death (D). The vertical dashed lines indicate the median lethal temperature (LT_{50} = 81 °C) and the 99% probabilistic suppression threshold (LT_{99} = 87.2 °C) confirming that macroscopic lethality requires thermodynamic inputs exceeding 80 °C.

3.6. Morphological Cellular Damage Analysis by Scanning Electron Microscopy (SEM)

In contrast, micrographs of treated samples (Figure 8b) revealed severe structural damage. Spores exhibited a quantified reduction in average diameter alongside loss of turgor, extreme shrinkage, and topographic deformation. Mycelial structures showed hyphal discontinuity and collapsed segments. Collectively, SEM evidence supports the physical mechanism underlying the profound loss of viability, demonstrating that the treatment severely compromises cellular integrity, rendering standard pathogenic recovery highly unlikely.

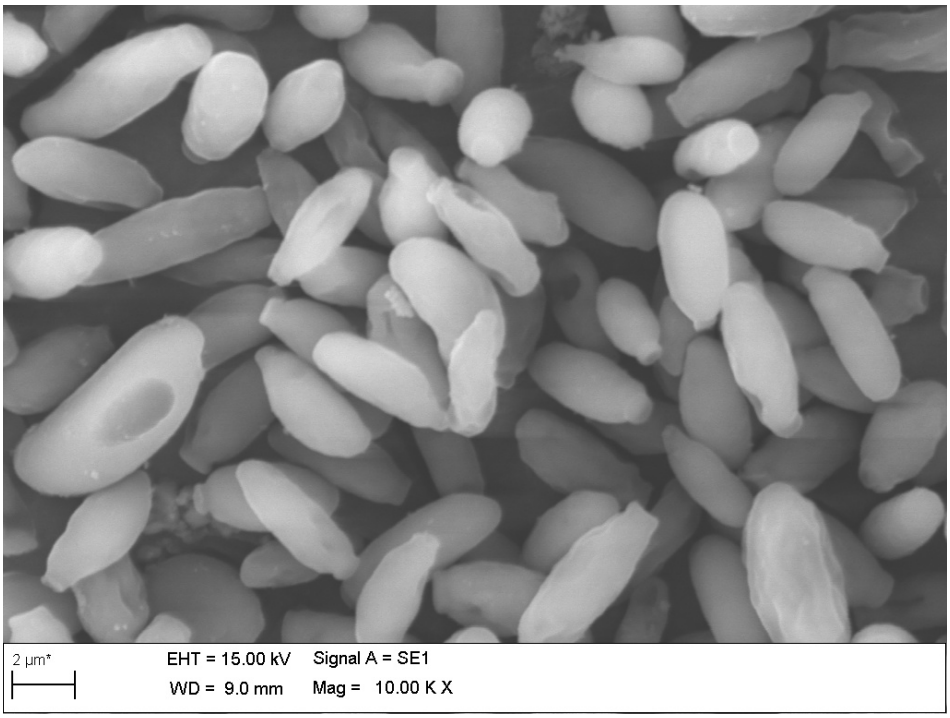

(**a**)

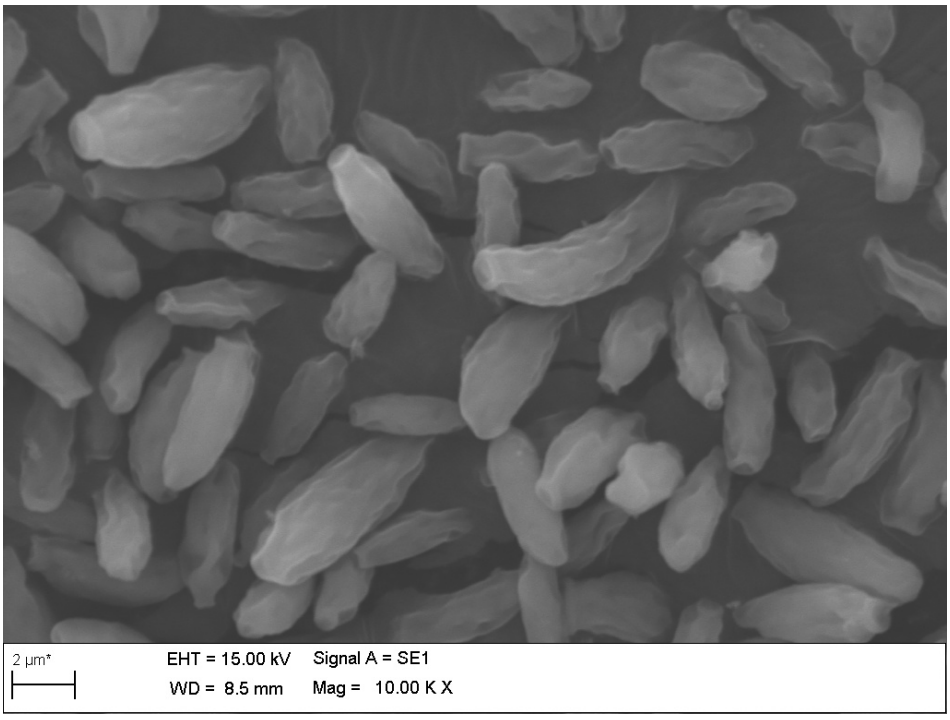

(**b**)

Figure 8. SEM micrographs of *F. solani*. (**a**) Control (untreated): untreated microorganisms showing intact macroconidia and hyphal integrity. Macroconidia display smooth surfaces with well-defined septa and the typical falcate morphology, while hyphae appear continuous with relatively uniform diameter and regular contours, with no evidence of collapse or rupture, consistent with high viability. (**b**) Treated (>80 °C, Outcome: D): after lethal microwave exposure (>80 °C) showing irreversible ultrastructural collapse consistent with Death (D). Treated macroconidia exhibit loss of turgor, extreme shrinkage, and wrinkled surfaces, while hyphae show discontinuity, irregular diameters, and collapsed segments, indicating structural failure incompatible with recovery. (The asterisk (*) on the scale bar is a software display indicator and does not affect calibration; the 2 µm measurement is exact for morphometric analysis).

3.6.1. Structural Integrity of the Untreated Control

In the untreated control (Figure 8a), macroconidia retained their typical morphology: a smooth surface, a well-defined septa, and a falcate (slightly curved) shape, consistent with high turgor pressure and intact cellular envelopes. Similarly, mycelial structures displayed continuous filaments, relatively uniform diameter, and regular contours, with no evidence of rupture or collapse—indicating stable cell walls and membranes and, therefore, high biological viability.

3.6.2. Cytological Collapse Induced by Irradiation (Death, D)

In contrast, micrographs of treated samples (Figure 8b) revealed severe and structural damage in both structure types. Spores exhibited loss of turgor, extreme shrinkage, and topographic deformation (wrinkled surface), consistent with dehydration and generalized cell-wall collapse. Mycelial structures showed hyphal discontinuity, irregular diameters, collapsed segments, and rough surfaces, indicating marked structural failure. This pattern of physical degradation is associated with the high heating rate induced by microwaves under lethal conditions, which promotes abrupt intracellular water vaporization and denaturation of structural proteins that support the fungal wall. Collectively, SEM evidence supports the physical mechanism underlying the Death (D) outcome—defined as the complete absence of fungal growth—demonstrating that the treatment not only limits pathogen metabolism but also compromises cellular integrity in a manner incompatible with recovery or future viability.

3.6.3. Quantitative Morphometric Alterations

Quantitative morphometric analysis of the SEM micrographs revealed dimensional alterations in the spores following microwave irradiation. The average transverse width exhibited a significant decrease, reducing from 2.12 ± 0.50 µm in the control to 2.03 ± 0.50 µm in the treated group. Concurrently, the longitudinal dimension exhibited an increase, going from 3.49 ± 0.94 µm in the control to 4.10 ± 1.09 µm after treatment, consistent with the loss of turgor and structural deformation observed in Figure 8b. A summary of these morphometric parameters is presented in Table 5.

Table 5. Summary of morphometric parameters obtained from untreated and experimentally treated *F. solani* spores via SEM micrograph analysis.

Treatment Group	Parameter	Mean ± SD (µm)	Range (µm)	*n*
Untreated Control	Spore Length	3.49 ± 0.94	2.00–5.16	12
	Spore Width	2.12 ± 0.50	1.59–3.23	12
Microwave-Treated	Spore Length	4.10 ± 1.09	2.29–6.26	12
	Spore Width	2.03 ± 0.50	1.41–2.78	12

Note: Morphometric values are expressed as the mean ± standard deviation (SD) of $n = 12$ representative spores per treatment group. Measurements were digitally calibrated using the internal 2 µm SEM scale bar (k = 0.0290 ± 0.0008 µm/px). The observed significant decrease in the transverse axis (Spore Width), alongside the elongation of the longitudinal axis, quantitatively reflects the severe topographic deformation, lateral shrinkage, and loss of cellular turgor induced by the lethal thermal shock.

Statistical comparison using an independent-samples Student's *t*-test confirmed a significant decrease in the transverse width of the spores post-treatment. A comparison of the morphometric data reveals that while the mean transverse width reduced, its standard deviation remained constant, indicating a uniform and significant lateral shrinkage across the sampled population. Conversely, the longitudinal axis exhibited the inverse behavior, showing a highly variable elongation trend (increasing by 17.6% on average) accompanied by an increase in data dispersion.

3.7. Thermal Response of Mycelial Plugs on Solid Media

3.7.1. Fungal Persistence in Sublethal Ranges (40–80 °C)

Heating kinetics associated with *F. solani* mycelial plugs (average dimensions: 5 mm in length × 2 mm in diameter) placed on PDA in Petri dishes (Figure 4) showed no biological efficacy within sample surface temperature ranges up to 80 °C. Despite the progressive increase in surface temperature during exposure, all experimental units evaluated at 60–70 °C and 70–80 °C exhibited a Reduced Growth Rate (RGR) after subsequent incubation. These results indicate that the thermal energy accumulated below 80 °C produces only a transient fungistatic effect, insufficient to overcome the pathogen's thermotolerance.

3.7.2. Lethal Inactivation and Operational Efficiency (>80 °C)

In contrast, the eradicative capacity of the treatment was confirmed once thermal profiles exceeded the 80 °C surface-temperature threshold (Figure 5). When surface temperature was stabilized within the 80–90 °C and 90–100 °C ranges, Death (D)—defined as the complete absence of fungal growth—was consistently recorded. Under these lethal conditions, no regrowth was observed during subsequent incubation, supporting a severe loss of viability. The 210 W treatment generated steeper surface-heating slopes than 140 W, enabling lethal temperatures (>80 °C) to be reached with shorter exposure times and improving operational efficiency without compromising the inactivation outcome.

4. Discussion

4.1. Redefining the Lethal Threshold for Fusarium solani

Experimental observation combined with robust statistical modeling definitively redefines the thermal tolerance limits of Fusarium solani under microwave irradiation. Temperatures within the 70–80 °C band induce a highly significant fungistatic effect, characterized by a Reduced Growth Rate (RGR), but remain strictly sublethal. Profound suppression (D) strictly requires breaching the 80 °C barrier. The computed LT_{50} (81.0 °C) and LT_{99} (87.2 °C) metrics confirm that the critical destabilization of the fungal cell wall demands thermal inputs closely approaching the boiling point of the intracellular aqueous matrix, effectively overwhelming the pathogen's primary adaptive stress responses, even if a marginal fraction retains minimal residual viability.

The symptomology observed during the in vivo assay—characterized by necrotic dark lesions, rapid cuticular expansion, and prominent white-cottony mycelial growth—strongly aligns with the pathogenic behavior reported for emerging Fusarium strains affecting Theobroma cacao pods under humid postharvest and tropical conditions [5]. This confirms that the CHA1 isolate possesses active, aggressive colonization capabilities that justify physical postharvest interventions.

4.2. Heating Rate (H_r) as a Decisive Engineering Parameter

From an engineering perspective, lethality is tightly coupled not only with the final temperature but with the heat transfer kinetics and the specific heating rate (H_r). Low heating rates (e.g., 0.085–0.167 °C/s at 140 W) grant the pathogen an extended residence time within sublethal conditions, which may trigger transient thermotolerance mechanisms. In contrast, maximizing H_r to 0.381 °C/s via 210 W microwaves overwhelms the biological adaptation window. As noted by Tang [38], rapid dielectric heating generates violent intracellular vaporization. This physical phenomenon justifies the irreversible structural collapse and acute dehydration of the macroconidia observed in the SEM micrographs. Prioritizing high heat transfer rates significantly reduces the heating time required to reach a specific target temperature, providing a scalable thermodynamic framework for continuous unit operations [10,39].

A Student's t-test analysis confirmed that increasing the microwave power to 210 W significantly maximized the heating rate (H_r) compared to the 140 W settings ($t = 29.17$, $p < 0.0001$). This highly significant kinetic difference validates the engineering hypothesis that higher electromagnetic energy inputs successfully minimize thermal residence time. Consequently, these parameters position high-power microwave treatments as a viable alternative or adjuvant unit operation to existing postharvest interventions, such as chemical control, biological interventions during postharvest [40], or conventional convective heating. It is important to note that while this study establishes rapid heating rates via microwave irradiation, direct experimental comparisons with conventional heating controls were not performed; thus, future studies should comparatively evaluate these kinetics against traditional thermal methods to fully quantify the operational advantages.

4.3. A Temperature-Defined Lethal Threshold Resolves Parameter Ambiguity in MW Fungal Control

This study identifies a practical lethal threshold for *F. solani* in cocoa-relevant plate assays: consistent lethality occurs once surface temperature exceeds 80 °C, while temperatures up to 80 °C produce only RGR. A threshold-first interpretation improves reproducibility because MW efficacy depends on achieved thermal state rather than nominal time, particularly in heterogeneous matrices.

4.4. Biological Plausibility: FSSC Diversity and Virulence Genetics Justify a Threshold-Based Approach

Given the diversity and variable virulence mechanisms described for the FSSC, time-only prescriptions are unlikely to generalize across isolates. A temperature-verified threshold provides a defensible control specification that is robust to isolate-level heterogeneity and matrix variation.

4.5. Ultrastructural Validation Strengthens Inference Beyond Growth Endpoints

SEM confirms complete loss of turgor, extreme shrinkage, and discontinuity in macroconidia and hyphae under lethal conditions (Figure 8a,b), strengthening inference beyond plate regrowth endpoints. Turbidimetric monitoring over 120 h further supports this inference. Despite observing natural biological variability and statistical overlap during the early exponential phase, the complete separation of standard deviation bars by 120 h demonstrates a reliable and sustained suppression. This indicates that the lethal regime produces irreversible or deeply injurious effects that, while allowing a severely debilitated recovery (OD 0.4), are fundamentally incompatible with normal virulence and proliferation.

The quantitative morphometric changes further illustrate the physical impact of the thermal shock. Specifically, the longitudinal axis of the spores exhibited a notable average increase of 17.6% (reaching 4.10 μm compared to 3.49 μm in the control), while the transverse width experienced a corresponding reduction of 4.3% (decreasing to 2.03 μm from 2.12 μm in the control). Rather than maintaining uniform dimensions, this asymmetric dimensional shift—combining lateral shrinkage with longitudinal elongation—reflects the severe topographic deformation, loss of cellular turgor, and structural collapse induced by rapid intracellular water vaporization under lethal conditions. This pronounced morphological degradation permanently compromises cellular viability, corroborating the lethality consistently observed in the >80 °C treatments.

The kinetic analysis of cellular inhibition (Table 3) reveals a biphasic biological response to the electromagnetic thermal shock. At 48 h, the treatment achieves a maximum inhibition of 94.5%, corresponding to a drastic extension of the lag phase and severe acute cellular stress. However, the gradual decrease in inhibition to 62.2% by 120 h suggests

the activation of late-stage repair mechanisms in a heavily debilitated subpopulation. This kinetic behavior confirms that while achieving maximum suppression requires pushing surface temperatures beyond the LT_{99} threshold, sublethal exposures still inflict profound, long-lasting structural damage that successfully neutralizes the pathogen's primary infective vigor.

4.6. Throughput vs. Lethality: Power Governs Speed, Temperature Governs Outcome

The data support a clear engineering distinction: MW power primarily governs heating kinetics and operational throughput, whereas lethality is governed by surpassing the thermal threshold. Higher power (210 W) reduced time-to-lethal relative to 140 W (to reach 90–100 °C), enabling shorter thermal residence.

4.7. Positioning MW Within Integrated Management and the Cocoa Value Chain

A temperature-verified MW unit operation could complement integrated management by providing a standardized postharvest barrier less dependent on perfect field-level prophylaxis adoption. The power–time windows identified here offer actionable design inputs for scaling MW treatment while minimizing exposure time.

5. Conclusions

This study demonstrates the efficacy of continuous microwave irradiation as a physical method for the inactivation of *F. solani*, fundamentally establishing that macroscopic suppression is governed by both the final surface temperature and the heat transfer kinetics (H_r). The thermodynamic modeling definitively identified that the 70–80 °C thermal band induces only sublethal stress (Reduced Growth Rate), whereas severe cellular suppression strictly requires breaching the 80 °C threshold. The binomial logistic regression provided precise thermal indices, projecting the median lethal temperature (LT_{50}) at 81.0 °C and the 99% probabilistic suppression threshold (LT_{99}) at 87.2 °C. Furthermore, utilizing higher energy inputs (e.g., 210 W) maximizes the heat transfer rate, significantly reducing the heating time required to achieve these lethal target temperatures and overwhelming the pathogen's primary adaptive responses.

These results represent foundational, laboratory-scale in vitro data, while the established thermal kinetics and lethal thresholds provide a robust baseline for electromagnetic pathogen suppression, these parameters cannot be directly extrapolated to industrial environments. Following these findings, future scaled research must validate these thermodynamic models in vivo on intact, harvested cocoa pods to assess microwave penetration depth, heat dissipation within the heterogeneous fruit matrix, and the technical viability of integrating this unit operation into commercial postharvest management pipelines.

Author Contributions: Conceptualization, W.A.L.P.; methodology, W.A.L.P., O.A.N.M., H.F.G.-M. and N.A.M.C.; software, O.A.N.M. and H.F.G.-M.; validation, W.A.L.P., O.A.N.M., H.F.G.-M., N.A.M.C. and A.P.A.; formal analysis, W.A.L.P., H.F.G.-M. and N.A.M.C.; investigation, W.A.L.P., O.A.N.M., H.F.G.-M. and N.A.M.C.; resources, W.A.L.P., O.A.N.M., H.F.G.-M. and A.P.A.; data curation, W.A.L.P. and O.A.N.M.; writing—original draft preparation, W.A.L.P., O.A.N.M., H.F.G.-M., N.A.M.C. and A.P.A.; writing—review and editing, W.A.L.P. and O.A.N.M.; visualization, A.P.A.; supervision, W.A.L.P.; project administration, O.A.N.M.; funding acquisition, O.A.N.M. and A.P.A. All authors have read and agreed to the published version of the manuscript.

Funding: This research was funded by the Research Directorate of Fundación Universitaria Los Libertadores, Internal Research Call No. 13 of 2025, grant number ING-05-25.

Data Availability Statement: The original contributions presented in the study are included in the article; further inquiries can be directed to the corresponding author.

Acknowledgments: AI-assisted tools were used solely for language translation of portions of the manuscript from [original language] into English. The use of AI was limited to improving linguistic clarity and readability (translation and minor language refinement) and did not involve generating new scientific content, altering the meaning of the authors' text, producing results, performing analyses, or creating interpretations or conclusions. All scientific content, data, and conclusions were developed by the authors, who reviewed and verified the final wording for accuracy and fidelity to the original meaning.

Conflicts of Interest: The authors declare no conflicts of interest.

Abbreviations

The following abbreviations are used in this manuscript:

BLAST	Basic Local Alignment Search Tool
CI	Confidence Interval
CRD	Completely randomized design
D	Death
HMDS	Hexamethyldisilazane
IR	Infrared
ITS	Internal transcribed spacer
MW	Microwave
OD	Optical density
PDA	Potato dextrose agar
RGR	Reduced growth rate
SD	Standard deviation
SEM	Scanning electron microscopy
TEF1α	Translation elongation factor 1-alpha

References

1. Copetti, M.V.; Iamanaka, B.T.; Frisvad, J.C.; Pereira, J.L.; Taniwaki, M.H. Mycobiota of cocoa: From farm to chocolate. *Food Microbiol.* **2011**, *28*, 1499–1504. [CrossRef] [PubMed]
2. Parra Peñalosa, O.J.; Gallardo, R.A.V.; García-Contreras, R.; Hernández-Hernández, F.; Martínez, E.C. Morpho-molecular characterization of fungi in harvested fruits of *Theobroma cacao* L. *Agron. Colomb.* **2025**, *43*, e120512. [CrossRef]
3. Coleman, J.J. The Fusarium solani species complex: Ubiquitous pathogens of agricultural importance. *Mol. Plant Pathol.* **2016**, *17*, 146–158. [CrossRef] [PubMed]
4. Ploetz, R.C. Fusarium-Induced Diseases of Tropical, Perennial Crops. *Phytopathology* **2006**, *96*, 648–652. [CrossRef] [PubMed]
5. Dávila, L.; Rodriguez, E.; Villabona-Gelvez, A.; Huguet-Tapia, J.C.; Zuluaga, P. Integrative genomic and pathogenicity analyses reveal emerging *Fusarium* threats to cacao in Colombia. *Physiol. Mol. Plant Pathol.* **2026**, *145*, 103368. [CrossRef]
6. Rosmana, A.; Hikmawati; Zulfikar, M.; Asman; Fadillah, D. Identification of a Disease on Cocoa Caused by Fusarium in Sulawesi. *Pelita Perkeb. (Coffee Cocoa Res. J.)* **2013**, *29*, 210–219. [CrossRef]
7. Gunaedi, T.; Tanjung, R.H.R.; Manwan, S.W. DNA Barcoding of Cacao Pod Rot Fungi in Papua Province. *East Asian J. Multidiscip. Res.* **2024**, *3*, 671–680. [CrossRef]
8. Delgado-Ospina, J.; Molina-Hernández, J.B.; Chaves-López, C.; Romanazzi, G.; Paparella, A. The Role of Fungi in the Cocoa Production Chain and the Challenge of Climate Change. *J. Fungi* **2021**, *7*, 202. [CrossRef] [PubMed]
9. Zhang, H.; Ge, L.; Ma, L.; Chen, K.; Jiang, S. Effects of microwave treatment on postharvest decay of fruits: A review. *Stewart Postharvest Rev.* **2009**, *5*, 1–7. [CrossRef]
10. Luo, K.; Tao, Y.; Yang, H.; Yan, B.; Zhang, H.; Chen, W. Recent advances in microwave inactivation of foodborne pathogens: Key factors, mechanisms, and future perspectives. *Trends Food Sci. Technol.* **2025**, *165*, 105338. [CrossRef]
11. Akhila, P.P.; Sunooj, K.V.; Aaliya, B.; Navaf, M.; Sudheesh, C.; Sabu, S.; Sasidharan, A.; Mir, S.A.; George, J.; Khaneghah, A.M. Application of electromagnetic radiations for decontamination of fungi and mycotoxins in food products: A comprehensive review. *Trends Food Sci. Technol.* **2021**, *114*, 399–409. [CrossRef]
12. Berni, E.; Brutti, A. Electromagnetic radiations and their effect on filamentous fungi and mycotoxins: Recent advances and perspectives. *Curr. Opin. Food Sci.* **2023**, *52*, 101073. [CrossRef]
13. da Silva, A.C.; Sarturi, H.J.; Dall'Oglio, E.L.; Soares, M.A.; de Sousa, P.T.; de Vasconcelos, L.G.; Kuhnen, C.A. Microwave drying and disinfestation of Brazil nut seeds. *Food Control* **2016**, *70*, 119–129. [CrossRef]

14. Zhang, H.; Zheng, X.; Su, D. Postharvest control of blue mold rot of pear by microwave treatment and *Cryptococcus laurentii*. *J. Food Eng.* **2006**, *77*, 539–544. [CrossRef]
15. Abdelrhim, A.S.; Dawood, M.F.A.; Galal, A.A. Hydrogen peroxide-mixed compounds and/or microwave radiation as alternative control means against onion seed associated pathogens, *Aspergillus niger* and *Fusarium oxysporum*. *J. Plant Pathol.* **2022**, *104*, 49–63. [CrossRef]
16. Soriano-Martín, M.L.; Porras-Piedra, A.; Porras-Soriano, A. Use of microwaves in the prevention of *Fusarium oxysporum* f. sp. *melonis* infection during the commercial production of melon plantlets. *Crop Prot.* **2006**, *25*, 52–57. [CrossRef]
17. Basaran, P.; Akhan, Ü. Microwave irradiation of hazelnuts for the control of aflatoxin producing *Aspergillus parasiticus*. *Innov. Food Sci. Emerg. Technol.* **2010**, *11*, 113–117. [CrossRef]
18. Chandravarnan, P.; Agyei, D.; Ali, A. Green and sustainable technologies for the decontamination of fungi and mycotoxins in rice: A review. *Trends Food Sci. Technol.* **2022**, *124*, 278–295. [CrossRef]
19. Tian, T.; Zhang, B.; Chen, S.; Tao, T.; Liu, Q.; Liu, B.; Yuan, J.; Ding, C. Characterization of differences between microwave and traditional thermal sterilization to prevent fungal spoilage during storage of high-moisture paddy rice. *Cereal Chem.* **2020**, *98*, 154–163. [CrossRef]
20. Mao, Y.; Gerrow, A.; Ray, E.; Diaz Perez, N.; Edler, K.; Wolf, B.; Binner, E. Lignin recovery from cocoa bean shell using microwave-assisted extraction and deep eutectic solvents. *Bioresour. Technol.* **2023**, *372*, 128680. [CrossRef] [PubMed]
21. Petronaitis, T.; Brodie, G.; Simpfendorfer, S.; Flavel, R.J.; Warwick, N.W.M. Dielectric properties of cereal stubble infected with *Bipolaris sorokiniana*, *Fusarium pseudograminearum* and *Pyrenophora teres* in the microwave frequency range. *J. Microw. Power Electromagn. Energy* **2022**, *56*, 219–237. [CrossRef]
22. Villamizar-Gallardo, R.; Osma Cruz, J.F.; Ortíz-Rodríguez, O.O. Fungicidal effect of silver nanoparticles on toxigenic fungi in cocoa. *Pesqui. Agropecu. Bras.* **2016**, *51*, 1929–1936. [CrossRef]
23. Lemarcq, V.; Sioriki, E.; van de Walle, D.; Dewettinck, K. Influence of convection and microwave roasting on roasting degree, microstructure and aroma profile of cocoa beans. *Eur. Food Res. Technol.* **2022**, *248*, 2383–2392. [CrossRef]
24. Lemarcq, V.; Monterde, V.; Tuenter, E.; Van de Walle, D.; Pieters, L.; Sioriki, E.; Dewettinck, K. Flavor diversification of dark chocolate produced through microwave roasting of cocoa beans. *LWT* **2022**, *159*, 113198. [CrossRef]
25. Maghfiroh, A.D.; Yanti, R.; Hidayat, C. Microwave-assisted unfermented cocoa bean: Improving flavor precursor after acetic acid submersion. *J. Food Sci. Technol.* **2024**, *61*, 279–289. [CrossRef] [PubMed]
26. Alean, J.; Chejne, F.; Maya, J.C.; Camargo-Trillos, D.; Ramírez, S.; Rincón, E.; Rojano, B. Evolution of the porous structure of cocoa beans during microwave drying. *Dry. Technol.* **2020**, *38*, 1313–1322. [CrossRef]
27. Correa-Abril, J.; Stahl, U.; Cabrera, E.V.; Parra, Y.J.; Vega, M.A.; Taamalli, S.; Louis, F.; Rodríguez-Díaz, J.M. Adsorption dynamics of Cd^{2+}(aq) on microwave-synthetized pristine biochar from cocoa pod husk: Green, experimental, and DFT approaches. *iScience* **2024**, *27*, 109958. [CrossRef] [PubMed]
28. Pattanakitjaroenchai, S.; Pitsawong, P.; Khat-Udomkiri, N. Exploration of cosmetic bioactive compounds from cocoa bean shell using polyol-based microwave-assisted extraction: Cytotoxicity, anti-tyrosinase, and anti-melanogenesis properties. *Curr. Res. Green Sustain. Chem.* **2025**, *10*, 100454. [CrossRef]
29. Gomez, P.; Reyes, C.; Figueroa, J.G. Microwave-Assisted Extraction of Phenolic Compounds from Cocoa Pod Husk: Process Optimization and Impact of Drying Temperature on Bioactive Recovery. *Molecules* **2025**, *30*, 3497. [CrossRef] [PubMed]
30. Castillo-Reyes, F.; De León-Juárez, E.; Nery-Flores, S.D.; Flores-Gallegos, A.C.; Campos-Muzquiz, L.G.; Ascacio-Valdés, J.A.; Rodríguez-Herrera, R. Polyphenols extraction from creosote bush, tarbush, and soursop using ultrasound-microwave and their effect against *Alternaria alternata* and *Fusarium solani*. *Rev. Mex. Fitopatol.* **2022**, *40*, 349–376. [CrossRef]
31. Gardes, M.; Bruns, T. ITS primers with enhanced specificity for basidiomycetes: Application to the identification of mycorrhizae and rusts. *Mol. Ecol.* **1993**, *2*, 113–118. [CrossRef] [PubMed]
32. Vilgalys, R. Phylogenetic implications of generic concepts in fungal taxonomy: The impact of molecular systematic studies. *Mycol. Helv.* **1994**, *6*, 73–91.
33. Yadav, D.N.; Anand, T.; Sharma, M.; Gupta, R.K. Microwave technology for disinfestation of cereals and pulses: An overview. *J. Food Sci. Technol.* **2014**, *51*, 3568–3576. [CrossRef] [PubMed]
34. Szopińska, D.; Dorna, H. The Effect of Microwave Treatment on Germination and Health of Carrot (*Daucus carota* L.) Seeds. *Agronomy* **2021**, *11*, 2571. [CrossRef]
35. Sun, X.; Zhao, C.; Yang, S.; Ma, H.; Zhai, C. Simulations and Experiments of Soil Temperature Distribution after 2.45 GHz Long-Term Microwave Treatment. *Agriculture* **2022**, *12*, 909. [CrossRef]
36. Hameed, T.; Motsi, N.; Bignell, E.; Tanaka, R.J. Inferring fungal growth rates from optical density data. *PLoS Comput. Biol.* **2024**, *20*, e1012105. [CrossRef] [PubMed]
37. Valdramidis, V.P.; Geeraerd, A.H.; Van Impe, J.F. Stress-adaptive responses by heat under the microscope of predictive microbiology. *J. Appl. Microbiol.* **2007**, *103*, 1922–1930. [CrossRef] [PubMed]
38. Tang, J. Unlocking potentials of microwaves for food safety and quality. *J. Food Sci.* **2015**, *80*, E1776–E1793. [CrossRef] [PubMed]

39. Chandrasekaran, S.; Ramanathan, S.; Basak, T. Microwave food processing—A review. *Food Res. Int.* **2013**, *52*, 243–261. [CrossRef]
40. Sukmawati, D.; Husna, S.N.A.; Firhandini, A.; Susilowati, D.N.; Setiarto, R.H.B.; Anshory, L.; Anggadhania, L.; Acheampong, M.A.; Enshasy, H.A.E. Biocontrol Potential and Mechanisms of Cocoa-Fermentation Yeasts Against Fungal Pathogens of Cocoa Pods. *Biointerface Res. Appl. Chem.* **2025**, *15*, 66. [CrossRef]